

# Causal Perception Inspired Representation Learning for Trustworthy Image Quality Assessment

Lei Wang, Desen Yuan

University of Electronic Science and Technology of China

wangleiuestc@outlook.com, desenyuan@gmail.com

## Abstract

Despite great success in modeling visual perception, deep neural network based image quality assessment (IQA) still remains unreliable in real-world applications due to its vulnerability to adversarial perturbations and the inexplicit black-box structure. In this paper, we propose to build a trustworthy IQA model via Causal Perception inspired Representation Learning (CPRL), and a score reflection attack method for IQA model. More specifically, we assume that each image is composed of Causal Perception Representation (CPR) and non-causal perception representation (N-CPR). CPR serves as the causation of the subjective quality label, which is invariant to the imperceptible adversarial perturbations. Inversely, N-CPR presents spurious associations with the subjective quality label, which may significantly change with the adversarial perturbations. To extract the CPR from each input image, we develop a soft ranking based channel-wise activation function to mediate the causally sufficient (beneficial for high prediction accuracy) and necessary (beneficial for high robustness) deep features, and based on intervention employ minimax game to optimize. Experiments on four benchmark databases show that the proposed CPRL method outperforms many state-of-the-art adversarial defense methods and provides explicit model interpretation.

## 1. Introduction

The rapid growth of image data on the Internet has made the automatic evaluation of image quality a vital research and application topic. Objective image quality assessment (IQA) methods can be divided into three categories based on the availability of the original undistorted images: full-reference (FR), reduced-reference (RR), and no-reference/blind (NR/B). Among them, BIQA model is a challenging computational vision task, which mimics the human ability to judge the perceptual quality of a test image without requiring the original image content[19, 22, 26,

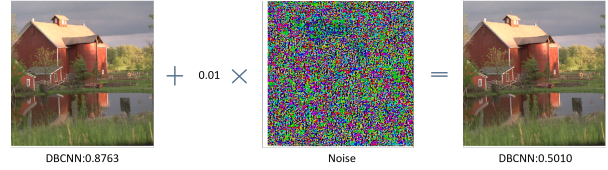


Figure 1. Demonstration of IQA model adversarial example generation). By adding an imperceptible perturbation, we can drastically change the predicted score of an IQA model for an image.

44, 53]. However, existing BIQA methods are not reliable, and minor perceptual attacks can fool the quality evaluator to produce incorrect output. This vulnerability affects the security issues, resulting in lower reliability of IQA[55]. As shown in Fig 1, after adding minor perturbations, the prediction results of the deep IQA model showed significant errors while the human eye does not perceive the change in quality. In image classification, this is known as adversarial attack (e.g., ‘norm constrained attack’). A reliable IQA model should not be overly sensitive to adversarial attacks, that is, be adversarially robust[12, 13, 20].

The prevalent approach to adversarial robustness is still empirical adversarial training and its variants. However, adversarial training is a form of “passive immunity” that cannot adapt to dynamic attacks. Model-based denoising defense is another important defense strategy. However, in quality assessment tasks, denoising models may backfire and have adverse effects. This is because the denoising operation itself alters image quality without affecting image semantics[46]. slight interference from the picture will not affect the perceptual quality of the human eye. The specific reason can be related to the all or nothing principle [14]. Recently, researchers have analysed adversarial examples from non-robust features and robust features, and demonstrated that robust features can still provide precise accuracy even in the presence of adversarial perturbations[12]. Researchers believe that the high-dimensional dot product operation and multi-layer structure of DNN form a dense mixture so that small changes in features can accumulate [1,

and cause excessive Lipschitz constant[54].

We propose a new way to understand the IQA task by using a causal approach. We use a causal framework that shows how the images in the IQA dataset are produced by three factors: reference images, causal perception representation (CPR) and non-causal perception representation (N-CPR). We say that N-CPR are confounders that do not affect image quality but can create false correlations. These confounders can make the model predictions wrong, and they can be any feature that is related to some labels, such as local texture, small edges, and faint shadows. Fig. 3 illustrates the structural causal model (SCM) that we use to describe how the data for the IQA dataset is generated. The normal IQA training and testing can be seen as changing the reference image  $R$  while keeping the N-CPR fixed. In this case, the non-robust features are stable, so the model can work well from the training to the test scenario. But in an adversarial scenario, someone can change the image quality by changing the N-CPR without changing how the image looks. This is a problem, because the current IQA networks cannot tell the difference. They do not use any prior knowledge to remove the confounders and stop the false correlations.

we propose to build a trustworthy IQA model via Causal Perception inspired Representation Learning (CPRL). specifically, IQA models that only depend on statistical associations are inadequate and unreliable, our method uses a causal intervention to break the false correlations and find the true cause of image quality. To extract the CPR from each input image, we develop a soft ranking-based channel-wise activation function to mediate the causally sufficient (beneficial for high prediction accuracy) and necessary (beneficial for high robustness) deep features. We train this module with the probability of necessity and sufficiency (PNS) risk[39, 42, 49]. Finally, we systematically compare the performance of our method with existing methods in different scenarios. Experimental results show that channel activation improves the accuracy of image quality significantly.

## 2. Related Work

### 2.1. Image quality assessment

Image quality assessment aims to obtain an objective model[44] to predict the image quality, making it close to the subjective quality score. Interpretable and reliable structural similarity (SSIM)[44] and peak signal-to-noise ratio (PSNR) are favored by researchers as a reference image quality method. However, researchers have been looking for methods similar to the human visual system(HVS) that do not require reference pictures which have been called no-reference(NR) IQA methods[43]. Due to the lack of information on reference pictures, naturally, the researchers used

the statistical information of pictures as a reference, called natural scene statistics (NSS)[7], and proposed Natural Image Quality Evaluator (NIQE) [27]. Benefiting from the development of deep learning, some learning-based image quality models [3, 23, 56] have obtained stronger performance than traditional quality evaluation methods[25] due to the powerful feature extraction capabilities of convolution kernels[11]. In order to explore more feature expression capabilities, researchers proposed many other methods based on Generative adversarial network [22], Variational Auto-Encoder [41], and Transformers [50]. However, powerful feature representation is difficult to explain, so some researchers try to figure out whether the quality evaluation is decoupled from the content[18]. Therefore, this paper focuses on the robustness exploration of deep IQA models, and dedicates to discovering efficient ways to improve the robustness of IQA models.

### 2.2. Vulnerability of deep neural networks

The vulnerability of Deep Neural Networks is believed to be due to the differences between the features extracted by the model and the human visual system [12]. So small changes can make deep models ineffective [9, 36]. The most classical anti-sample attack method, Fast Gradient Sign Method (FGSM)[10], which is based on gradient attack, has the following form:

$$x^{\text{adv}} := x + \varepsilon \cdot \text{sign}(\nabla_x L(h(x), y_{\text{true}})) \quad (1)$$

where  $x^{\text{adv}}$  is the adversarial example, which equals to the original sample plus a small perturbation.  $\varepsilon$  The direction of the perturbation is determined by the gradient of the predictor output  $h(x)$  and the label  $y$  with respect to the loss  $L$ . The magnitude of the perturbation is given by  $\varepsilon$ . Researchers found that the parameters of the neural network have a dense mixture of terms [1], and adversarial training is doing feature purification which alleviates vulnerability.

### 2.3. Adversarial robust models

A more robust model is not only more consistent with human perceptual properties[6, 40], but also increases the ability to generalize outside the domain[34]. From the point of view of data preprocessing, Feature Squeezing [47] distinguishes between adversarial and clean samples by reducing the color bit depth of each pixel. From the point of view of feature extraction, Feature denoising [46] reduces noise in latent features. from the empirical results, it can be seen that the feature spectrum is purer than the original deep network. Cisse proposed Parseval networks [5], a layerwise parameters regularization method for reducing the network's sensitivity to small perturbations by carefully controlling its global Lipschitz constant. Qin proposed a Local Linearization regularizer [31] that encourages the loss

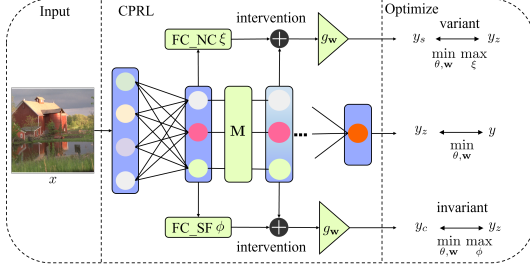


Figure 2. The CPRL module. We simply use this module to replace partial ReLU layers in the ResNet backbone to perform the IQA task.

to behave linearly in the vicinity of the training data. Kannan introduce enhanced defenses using a technique called logit pairing [15], a method that encourages logits for pairs of clean examples and their adversarial counterparts to be similar. All the above methods add additional constraints, such as controlling the Lipschitz constant to suppress the amplification effect of the network, or constraining the local linearity of features, or generating a purpose for feature alignment.

## 2.4. Causality inference

Various methods have been proposed to achieve causal inference, such as Matching Methods[35], Propensity Score based Methods[58], and Reweighting Methods[17, 33]. However, the balancing methods are not applicable in adversarial scenarios, because they mostly rely on the assumptions that the dataset is sufficient while non-perceptual representation are observed in natural images. Moreover, for high-dimensional images, there is not enough data for statistical analysis of causal estimation. Recently, some researchers have leveraged causal inference tools to optimize models from observable high-dimensional data [42, 49, 57]. Correspondingly, many perspectives have emerged to understand adversarial robustness from causal inference [13, 16, 20, 38, 59]. Furthermore, researchers use causal inference to obtain more reliable representations[4, 21, 48].

## 3. Preliminaries

### 3.1. Trustworthy IQA in adversarial attack

To form a credible IQA task in adversarial scenarios, we assume that there is a dataset  $D$  consisting of tuples of images  $x_i$ , corresponding labels  $y_i$ , and reference images  $R_i$ . We can represent the data as  $D = \{(R_i, x_i, y_i)_{i=1}^N\}$ , where  $N$  is the number of samples. The IQA task can be divided into two types: no-reference (NR) and full-reference (FR), depending on whether a reference image is given or not. A scene is FR if the reference image is observable during both training and testing phases. If the reference image is

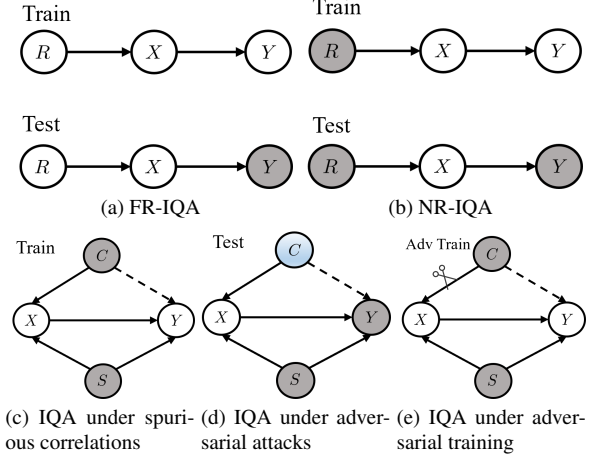


Figure 3. Causal graphs of IQA learning. Grey nodes represent unobserved variables. (a) Cause graphs of the traditional FR-IQA task during training and testing phases. (b) Cause graphs of the traditional NR-IQA task during training and testing phases. (c) Cause graphs of NR-IQA learning under spurious correlations during the training phase. Due to shortcut learning, the network model learns spurious correlations from the path  $X \leftarrow C \rightarrow Y$ . (d) Cause graphs of NR-IQA learning during the testing phase. The non-aware variables in blue are not from the same distribution as the training set. During the test phase, the distribution of confounding variables  $C$  in blue changes (adversarial attacks). (e) Cause graphs of NR-IQA adversarial learning. Adversarial training obtains new samples  $X$  by changing the confounding variable  $C$  and adding them to the training. Think of it as a backdoor intervention.

unobservable, then the scene is NR. The purpose of the adversarial attack defined in this paper is to find a perturbation  $\Delta x$  that reduces the network prediction quality score  $f(x)$ , which can be expressed as:

$$\arg \max_{\Delta x} L(y, f(x + \Delta x)), \text{ s.t. } d(\Delta x) \leq \epsilon, \quad (2)$$

where  $d$  is a signal fidelity measure,  $\epsilon$  is the bound of small perturbations, and  $L(\cdot, \cdot)$  represents the loss criterion for output and label. In practice, we define  $d$  as the  $\ell_\infty$ -norm measure  $\|\cdot\|_\infty$  and bounded by  $\epsilon = 1/255$ . Following the above formula, we clarify the differences between adversarial scenarios and traditional IQA tasks. Let  $P(\cdot)$  represent a marginal distribution. The difference between them is that the image  $X$  and its marginal distribution  $P(X)$  do not satisfy the assumption of independent and identically distributed (i.i.d.) samples, that is, for traditional IQA tasks,  $P(X_{\text{train}}) = P(X_{\text{test}})$ . For adversarial scenarios,  $P(X_{\text{train}}) \neq P(X_{\text{test}})$ .

### 3.2. Causal graphs in IQA learning

A causal graph is a directed acyclic graph in which nodes represent variables and directed edges represent the causal

relationship between two variables. We treat images, labels, reference images, causal perception representation (CPR) and non-causal perception representation (N-CPR) as nodes in a causal graph. Our causal graph reveals the underlying statistics of IQA learning, as we will show in the following sections. As shown in 3, we denote the image as  $X$ , the mean opinion score (MOS) as  $Y$ , CPR as  $S$ , and N-CPR as  $C$ . The edges are listed as follows:  $X \rightarrow Y$  means that MOS  $Y$  is derived from image  $X$ ;  $R \rightarrow X$  means that the reference image  $R$  has a causal influence on image  $X$ ;  $C \rightarrow Y$  with dotted line means that the N-CPR variable  $C$  has a spurious correlation with MOS  $Y$ ;  $C \rightarrow X$  means that the N-CPR variable  $C$  has a causal influence on image  $X$ ;  $S \rightarrow X$  means that the CPR variable  $S$  has a causal influence on image  $X$ ;  $S \rightarrow Y$  means that the CPR variable  $S$  has a causal influence on MOS  $Y$ . For traditional IQA learning in 3(a)(b), its causal graph contains the causal relationship between the image variable  $X$ , the label  $Y$ , and the reference image  $R$ . During the training phase of supervised learning, both the image  $X$  and the label  $Y$  are observable, and we use them to learn the causal effects in the model. But in the testing phase, only the image  $X$  and the causal path are known, and  $Y$  is the label to be predicted. For NR-IQA learning,  $R$  is unobservable, while for FR-IQA learning,  $R$  is observable. For the trustworthy IQA learning scenario, we model an unobserved variable, the non-perceptual variable  $C$ , and they are illustrated in 3(c). Their differences in the test phase are shown in 3(d). Due to changes in the non-perceptual variable  $C$ ,  $X$  may have an indirect effect on  $Y$  through the causal path  $X \leftarrow C \rightarrow Y$ , establishing a spurious correlation with  $C$ . The purpose of trustworthy IQA is to establish true quality-related correlations based on image quality evaluation, independent of non-perceptual variables.

## 4. Methodology

In this section, we present a causal framework to analyze the biases induced by non-perceptual features in IQA, a causal intervention method to eliminate them, and the implementation details and pipeline of our approach.

### 4.1. Non-perceptual-feature induced bias in IQA

According to the causal graph, we can explain why the IQA model fails in adversarial scenarios. We attribute this phenomenon to biases induced by non-perceptual features. In 3(c), the causal path  $X \leftarrow C \rightarrow Y$  is a fork structure, and this path is spurious because it is outside the causal path from  $X$  to  $y$ . Opening this path will create non-perceptual feature-induced biases and produce erroneous outcomes. We give a simple example to illustrate this point. A causal graph A country's per capita chocolate consumption  $\leftarrow$  Economic conditions  $\rightarrow$  Number of Nobel Prize winners There is a strong correlation between a country's

per capita chocolate consumption and its number of Nobel Prize winners. This correlation seems absurd because we cannot imagine winning a Nobel Prize for eating chocolate. A more plausible explanation is that more people eat chocolate in wealthy Western countries, and Nobel laureates are preferentially selected from these countries. But this is a causal explanation, which leads to the observed correlation between chocolate and Nobel Prizes. If we could control for the confounding factor of economic conditions and collect data on the poor economic conditions under which chocolate is rarely consumed, then we could come to the correct conclusion that chocolate consumption is not related to the number of Nobel Prize winners. In 3(e), The fork structural causal path  $X \leftarrow C \rightarrow Y$  can be causally intervened through backdoor adjustment to eliminate the bias induced by non-perceptual features in IQA and estimate the causal effect from  $X$  to  $Y$ . We can get the expression of  $P(Y|do(X))$  according to the backdoor criterion[30]:

$$P(Y | do(X)) = \sum_c P(Y | X, c)P(C) \quad (3)$$

We find that adversarial training can be understood as a backdoor adjustment to a simplified situation:

$$P(Y | do(X)) = P(Y | X, c_{adv})P(c_{adv}) + P(Y | X, c_{natural})P(c_{natural}) \quad (4)$$

For a single sample  $x$ , we convert the summation term into two samples. Natural samples and corresponding adversarial samples are added to the training to eliminate the dependence on  $c$ . In the loss function of adversarial training, the weighted values of adversarial samples and natural samples can be regarded as the prior probability of the above formula. However, adversarial training is only a passive defense strategy. We seek more advanced causal representations. The key idea is to utilize the probability of causation (POC) to systematically describe the importance of features.

### 4.2. Causal perception inspired representation learning for IQA

In this subsection, we introduce the score reflection attack method, and a novel channel-wise activation function based on soft ranking and a max-min game training strategy based on PNS, which aims to learn a causal representation that is both sufficient and necessary for the prediction. The overall framework is shown in 2.

Since image quality results value ranking, when we attack the image quality evaluation task, the aim is to invert the quality of image predictions (relative to the median value of 0.5) to interfere with the ranking, making the score gap larger, we called the score reflection attack:

$$x^{adv} := x + \varepsilon \cdot \text{sign}(\nabla_x \|h(x), \text{sign}(y_{true} - 0.5)\|_2) \quad (5)$$



We first compute a perceptual score  $\mathbf{M}$  for the feature  $f(x)$  and apply a nonlinear function  $g$  to the element-wise product of  $f(x)$  and  $\mathbf{M}$ :

$$y = g(f(x) \odot \mathbf{M}) \quad (6)$$

We use a sigmoid function to obtain  $\mathbf{M}$  from the sort index of  $f(x)$  with and bias term  $b$ , and Number of channels  $K$ :

$$M = \frac{1}{1 + e^{-(\text{sort}(f(x)) - K/2 + bK)}} \quad (7)$$

To ensure that the activated channels are both necessary and sufficient for the prediction, we adopt the probability of necessity and sufficiency (PNS) as a measure of causal relevance and optimize it during training[49]. PNS is defined by Pearl as the joint probability of a feature being both necessary and sufficient for the outcome:

$$PNS = P(Z = z, Y = y) \cdot PN + P(Z \neq z, Y \neq y) \cdot PS \quad (8)$$

where  $PN$  is the probability of necessity and  $PS$  is the probability of sufficiency, given by:

$$\begin{aligned} PN &\triangleq P(Y(Z \neq z) \neq y \mid Z = z, Y = y), \\ PS &\triangleq P(Y(Z = z) = y \mid Z \neq z, Y \neq y). \end{aligned} \quad (9)$$

However, computing counterfactual probabilities is intractable in general. Therefore, we use a lower bound of PNS as our objective, given by[42]:

$$PNS \geq P(Y = y \mid \text{do}(Z = z)) - P(Y = y \mid \text{do}(Z \neq z)) \quad (10)$$

We want to maximize PNS during training to make the feature causally relevant. To this end, we introduce two distributions that represent different interventions on the feature  $f(x)$ . Specifically, the distribution  $P^\phi(c \mid \mathbf{X} = \mathbf{x})$  samples a feature  $c$  that preserves the perceptual representation of  $f(x)$  but changes the non-perceptual representation. The distribution  $P^\xi(s \mid \mathbf{X} = \mathbf{x})$  samples a feature  $s$  that alters the perceptual representation of  $f(x)$  but keeps the non-perceptual representation intact. The distribution  $P^{\mathbf{w}}(y|z)$  gives the prediction of  $y$  given  $z$ . Then, we define the PNS risk as the sum of the sufficiency risk  $SF$  and the necessity risk  $NC$ :

$$R(\mathbf{w}, \phi, \xi) = SF(\mathbf{w}, \phi) + NC(\mathbf{w}, \xi) \quad (11)$$

The sufficiency risk  $SF$  measures the expected prediction error when  $z$  is sampled from the distribution that preserves the perceptual representation. The necessity risk  $NC$ , on the other hand, measures the expected prediction difference when  $z$  is sampled from the distribution that changes the perceptual representation. The risk increases when the representation contains less necessary and sufficient information.

We integrate the perceptual score term  $\mathbf{M}$  into the PNS risk, which leads to the final form of  $R(\mathbf{w}, \phi, \xi)$  as follows:

$$\mathbb{E}_{(\mathbf{x}, y) \sim \mathcal{D}} \mathbb{E}_{\mathbf{c} \sim P^\phi(\mathbf{c}|\mathbf{x})} \mathbb{E}_{\mathbf{s} \sim P^\xi(\mathbf{s}|\mathbf{x})} \|y_{\mathbf{c}} - y\|_2^2 - \|y_{\mathbf{s}} - y\|_2^2 \quad (12)$$

where  $y_{\mathbf{c}} = \text{sig}(g_{\mathbf{w}} \circ h_\phi(f(x), \mathbf{M}))$ ,  $y_{\mathbf{s}} = \text{sig}(g_{\mathbf{w}} \circ h_\xi(f(x), \mathbf{M}))$ . We use logistic regression as the prediction model and use the score term  $\mathbf{M}$  to control the intervention scope. Since we add the conventional regression loss at the end, we replace the labels here with the predicted values without intervention. We have  $y = \text{sig}(g_{\mathbf{w}}(f(x) \odot \mathbf{M}))$ . The function  $h_\phi(f(x), \mathbf{M})$  modifies the feature map  $f(x)$  by applying a non-linear transformation  $\text{FC}_\phi$  to the part that is masked by  $\mathbf{M}$  and adding it back to the original feature map. The function  $h_\xi(f(x), \mathbf{M})$  does the same thing but to the part that is masked by  $1 - \mathbf{M}$ , which is the complement of  $\mathbf{M}$ . Formally, we have:

$$\begin{aligned} c &= h_\phi(f(x), \mathbf{M}) = \text{FC}_\phi f(x) \odot (1 - \mathbf{M}) + f(x) \odot \mathbf{M}, \\ s &= h_\xi(f(x), \mathbf{M}) = \text{FC}_\xi f(x) \odot \mathbf{M} + f(x) \odot \mathbf{M}. \end{aligned} \quad (13)$$

We want to minimize PNS under any intervention distributions  $P^\xi$  and  $P^\phi$ , so the final loss is in the form of a min-max game. In other words, the intervention distribution at this time is equivalent to the worst-case adversarial distribution. We want to maximize the representativeness of PNS under this estimated adversarial distribution. We combine the regular MSE loss term with the PNS risk term to get the following optimization objective:

$$\min_{\theta, \mathbf{w}} \max_{\phi, \xi} \frac{1}{N} \sum_{i=0}^N \|g(f(x_i) \odot \mathbf{M}) - y_i\|_2^2 + R(\mathbf{w}, \phi, \xi) \quad (14)$$

In addition, spectral normalization[28] be applied to  $\phi$  and  $\xi$ , Prevent parameters from being too large. We summarize the overall CPRL training procedure in 1. The actual implementation adopts an alternating optimization scheme for updating the distribution parameters of the network, and leverages an intervention indicator to switch the output mode of the network and the optimization mode of the training pipeline.

## 5. Experiments

### 5.1. Settings

**datasets** We evaluate our method on four IQA datasets with different characteristics: LIVE and VCL, which contain artificially distorted images with a small size; and LIVEC and KONIQ, which contain naturally distorted images with a large size. KONIQ is the largest dataset with 10K images. Tab. 3 summarizes the details of the datasets.

**Comparison methods** We evaluate our proposed approach against three classic DNN-based IQA models and

Table 1. The SRCC and PLCC result of the existing IQA methods under 1/255 FGSM attack rates with clean training.

Datasets	VCL			LIVE			LIVEC			KONIQ		
	SROCC	PLCC	MSE	SROCC	PLCC	MSE	SROCC	PLCC	MSE	SROCC	PLCC	MSE
DBCNN [56]	0.1895	0.1677	0.0750	0.3216	0.3496	0.0658	-0.3211	-0.3502	0.1108	-0.1383	-0.1750	0.0420
NIMA [37]	-0.3869	-0.3838	0.1355	0.2278	0.2046	0.0740	-0.2417	-0.2656	0.1006	0.0805	0.0723	0.0290
ResNet [11]	-0.0892	-0.1045	0.0791	-0.0335	0.0700	0.0985	-0.1803	-0.2102	0.0809	-0.0831	-0.1109	0.0372
LWTA [29]	0.2999	0.3386	0.1659	0.5840	0.2550	0.1739	0.2438	0.2434	0.0721	0.6060	0.5816	0.0328
Denoise [46]	-0.3285	-0.3086	0.0971	-0.1447	-0.1082	0.1118	-0.2677	-0.2880	0.0826	0.1598	0.1522	0.0251
SAT [45]	0.3772	0.3409	0.0659	0.5100	0.5679	0.0528	-0.0666	-0.0555	0.0736	-0.3177	-0.3280	0.0581
CPRL	<b>0.9041</b>	<b>0.8841</b>	<b>0.0134</b>	<b>0.9022</b>	<b>0.8785</b>	<b>0.0123</b>	<b>0.7675</b>	<b>0.8173</b>	<b>0.0144</b>	<b>0.8228</b>	<b>0.8562</b>	<b>0.0052</b>

Table 2. The SRCC and PLCC result of the existing IQA methods under 1/255 PGD attack rates with clean training.

Datasets	VCL			LIVE			LIVEC			KONIQ		
	SROCC	PLCC	MSE	SROCC	PLCC	MSE	SROCC	PLCC	MSE	SROCC	PLCC	MSE
DBCNN	0.1078	0.0815	0.0724	0.3881	0.3364	0.0582	-0.3627	-0.4214	0.1188	0.0628	0.0317	0.0447
NIMA	-0.4032	-0.3996	0.1310	0.1652	0.2090	0.0688	-0.3841	-0.4130	0.1154	-0.0367	-0.0578	0.0340
ResNet	-0.0868	-0.1226	0.0801	0.2346	0.3368	0.0744	-0.2524	-0.2648	0.0818	-0.1245	-0.1507	0.0371
LWTA	0.3539	0.3387	0.2252	0.5887	0.1171	0.1780	0.2567	0.2454	0.0659	0.6291	0.6213	0.0346
Denoise	-0.2487	-0.2345	0.0888	0.0401	0.1459	0.0833	-0.2560	-0.2618	0.0744	0.0676	0.0576	0.0265
SAT	0.2437	0.2060	0.0784	0.4961	0.5534	0.0554	-0.2103	-0.1984	0.0853	-0.1507	-0.1578	0.0369
CPRL	<b>0.8694</b>	<b>0.8581</b>	<b>0.0176</b>	<b>0.8864</b>	<b>0.8530</b>	<b>0.0153</b>	<b>0.7295</b>	<b>0.7766</b>	<b>0.0173</b>	<b>0.8235</b>	<b>0.8542</b>	<b>0.0054</b>

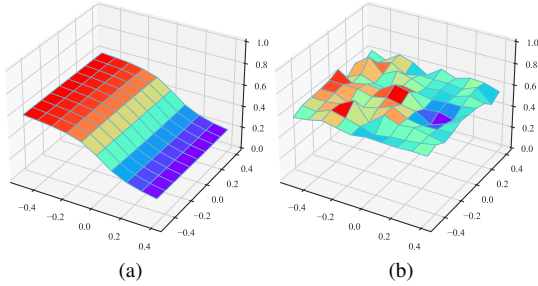


Figure 4. Output landscape on two-dimensional hyper-plane based on ResNet. specifically, one direction is the FGSM direction with a length of 1.0 pixels. Another direction is a random choice. Fig. 4a is the ResNet. Fig. 4b is the ResNet with CPRL. It can be found that the landscape is flat than original one. Regardless of the randomly selected perturbation direction or the perturbation direction of the adversarial attack, our landscape is flat, which empirically proves that CPRL is more robust.

three adversarial robust models. As the first work to study attack and defense in the IQA domain, we select the simplest and most effective defence method: the LWTA method [29], the denoising-based method [46], and SAT [45].

Table 3. Summary of IQA datasets.

Databases	# of Dist. Images	# of Dist. Types	Distortions Type
LIVE [32]	799	5	synthetic
VCL [52]	575	4	synthetic
LIVEC [8]	1,162	-	authentic
KONIQ [8]	10,073	-	authentic

**Attack methods** In order to verify the effectiveness of the proposed method, we choose the most classic adversarial sample attack methods FGSM and PGD[24], which are based on the gradient and are very representative.

**Metrics** We use three widely used metrics to evaluate the performances of the models, i.e., the Pearson’s Linear Correlation Coefficient (PLCC) [2], the Spearman’s Rank Order Correlation Coefficient (SROCC) [51], the Mean Square Error (MSE).

**Implementation** We split the data into training and testing sets at a 4:1 ratio randomly and saved the split-sequence to ensure the same division for all experiments. We also ensure that no source scene appears in both training and testing sets to avoid artificial inflation of the results. We re-

---

**Algorithm 1** CPRL Training Algorithm

---

**Input:** Training data  $\mathcal{D} = \{(x_i, y_i)\}_{i=1}^n$ .

**Output:** model parameter  $\{\theta, w, \phi, \xi\}$ . intervention symbol  $\text{int} = \text{None}$ . Number of iterations  $t = 0$ .

- 1: Initialize model with parameters  $\{\theta, w, \phi, \xi\}$ ,  $\text{int} == \text{None}$ .
  - 2: **while**  $t < T$  **do**
  - 3:   Calculate the model output and update phi  $\{\theta, w\}$  through minimize loss.
  - 4:   **if**  $\text{int} == \text{SF}$  **then**
  - 5:     Calculate the model output under  $c$  and update  $\phi$  through maximize loss,
  - 6:     Calculate the model output under  $c$  and update  $\{\theta, w\}$  through minimize loss,
  - 7:   **end if**
  - 8:   **if**  $\text{int} == \text{NC}$  **then**
  - 9:     Calculate the model output under  $S$  and update  $\xi$  through maximize loss,
  - 10:    Calculate the model output under  $S$  and update  $\{\theta, w\}$  through minimize loss,
  - 11:   **end if**
  - 12:    $t = t + 1$ , and change  $\text{int}$  by  $t$ .
  - 13: **end while**
- 

size the images in the training set to 320 randomly and crop them to  $320 * 320$  randomly. We resize and center crop the images in the test set. We assume that the cropped images have the same score as the original ones. We set the batch size to 16 and use AdamW with a learning rate of  $3e - 5$  for optimization. We initialize  $b$  to 0.4.

## 5.2. Evaluations

The existing IQA model and adversarial defence models have poor robustness, as shown by the results in Tab. 1 and Tab. 2. Their performance drops significantly with a small perturbation to the image under FGSM attack or PGD attack. The model's SRCC and PLCC values become negative, which means that the model gives inconsistent scores for slightly perturbed images. Our CPRL method enhances the robustness of the model and enables it to output more reliable scores for perturbed images. We can observe from Tab. 4 that our prediction performance on natural samples is also superior, compared with other methods. Please see the Appendix for more experimental results.

## 5.3. Ablation Studies

In this section, we conduct experiments to study the effect on our approach of 1) Whether to use PNS loss 2) channel activation rate 3) attack rate

**Impact of PNS risk** To examine the effect of PNS risk loss, we contrasted the results with channel activation alone. As shown in table Tab. 6, PNS achieves superior results. Both accuracy and robustness are enhanced.

**Impact of different attack rate** We conducted experiments to analyze them under different testing (different attack rates). As shown in Fig. 6, we set a uniform range of attack strengths to test the robustness of the proposed method. All models are all trained clean. Other methods suffer severe performance degradation under increasing attack intensity. By observing the results, it can be concluded that under different attack intensities, the proposed method can enhance the robustness of the model, and is superior to the comparison method.

**Impact of channel activation rate** To investigate the effect of the activation ratio controlled by parameter  $M$  on model performance, we conducted ablation studies on bias  $b$ . The experimental results are presented in table 5. We performed experiments on the LIVE dataset. The model is based on the ResNet50 network with channel activation and evaluated the robustness under different parameters. The experimental results reveal that the smaller the parameter  $b$ , the larger the activation ratio, which leads to better performance on clean samples, but lower robustness. We found that 0.4 is the optimal value for  $b$ .

## 5.4. Case Study

**Channel Activation value** Fig. 5 illustrates the bar plot of channel-wise activations for natural and adversarial test samples generated by FGSM attacks. For the vanilla ResNet model (trained on natural samples), the adversarial perturbations induce substantial deviations in the activation patterns of individual channels, resulting in the propagation of adversarial noise from the input layer to the output layer of the network. The ResNet model enhanced by CPRL exhibits more robustness than the vanilla ResNet in regions with high activation values. The optimization process ensures that regions with higher activation values are more causally salient, thus mitigating the output variation.

**landscape** Fig. 4 depicts the output landscape on a 2D hyperplane based on ResNet and CPRL. For vanilla ResNet, the landscape exhibits more variations, while CPRL shows more stability, and experiments confirm that CPRL is more robust.

## 6. Conclusion

In this paper, we propose to build a trustworthy IQA model through causal-aware inspired representation learning (CPRL), which only requires inserting the channel ac-

Table 4. The SRCC and PLCC result of the existing IQA methods without attack rates under clean training.

Datasets	VCL			LIVE			LIVEC			KONIQ		
	SRGCC	PLCC	MSE	SRGCC	PLCC	MSE	SRGCC	PLCC	MSE	SRGCC	PLCC	MSE
DBCNN	0.8967	0.8704	0.0277	0.9502	0.9274	0.0102	0.7157	0.7535	0.0191	0.8898	0.9116	0.0032
NIMA	0.9380	0.8890	0.0494	0.9396	0.9364	0.0105	0.7866	0.8292	0.0132	0.9014	0.9222	0.0029
ResNet	0.9234	0.9073	0.0115	0.8807	0.8212	0.0298	0.8341	0.8633	0.0121	0.8903	0.9123	0.0032
LWTA	0.2865	0.2907	0.2346	0.5259	0.1420	0.1788	0.2345	0.2521	0.0688	0.6384	0.6288	0.0375
Denoise	0.9317	0.9092	0.0158	0.8905	0.8238	0.0302	0.8191	0.8482	0.0131	0.8902	0.9155	0.0032
SAT	0.8021	0.7359	0.0315	0.8411	0.8146	0.0208	0.7005	0.7542	0.0193	0.8320	0.8680	0.0051
CPRL	0.9292	0.9222	0.0101	0.9266	0.9143	0.0104	0.8093	0.8620	0.0123	0.8567	0.8868	0.0042

Table 5. Performance comparison under different b on the LIVE dataset.

Datasets	clean			attack		
	SRCC	PLCC	MSE	SRCC	PLCC	MSE
b						
0.0	0.0100	0.0238	0.0534	-0.0249	-0.0663	0.0547
0.1	-0.2014	-0.2147	0.0576	-0.0296	-0.0155	0.0543
0.2	0.6798	0.6585	0.0400	0.5594	0.5303	0.0428
0.3	0.8154	0.7618	0.0375	0.7933	0.7353	0.0359
0.4	0.8560	0.8284	0.0350	<b>0.8432</b>	<b>0.7898</b>	<b>0.0427</b>
0.5	<b>0.8934</b>	<b>0.8646</b>	<b>0.0376</b>	-0.3538	-0.3671	0.1450

Table 6. Performance comparison on the LIVE dataset.

Datasets	clean			FGSM-1		
	SRCC	PLCC	MSE	SRCC	PLCC	MSE
Model						
CA	0.8743	0.8639	0.0163	0.8623	0.8478	0.0177
CA+PNS	0.9266	0.9143	0.0104	0.9022	0.8785	0.0123

tivation module before the regular activation function and adopts PNS risk for optimization. Extensive experiments on popular quality assessment datasets verify that our method can effectively improve the adversarial robustness of quality assessment models. The current work opens the door to trustworthy robust IQA models.

**Limitation and Future Work** Despite the strong performance of our model, it still suffers from some limitations. First, due to the more sophisticated optimization process, it requires additional optimization steps, which incur higher computational overhead. Moreover, achieving adversarial robustness through causal intervention is still an open challenge. The method of intervention through prediction in this paper may not be fully accurate, and there is still space for improvement. We intend to tackle these limitations and

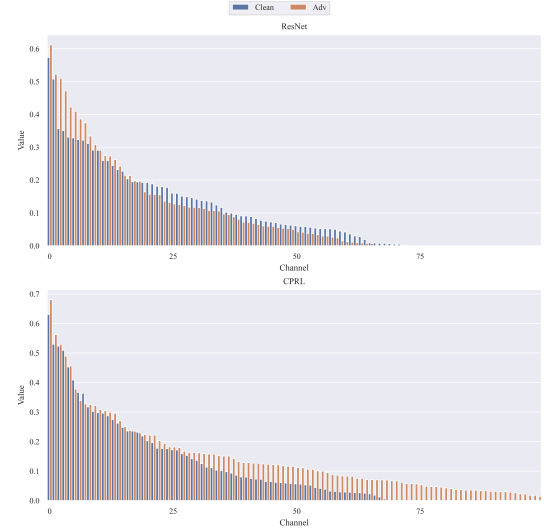


Figure 5. Channel activations value (y-axis) of intermediate layers of ResNet and CPRL models. In each figure, natural and adversarial test examples are shown respectively. The channels are arranged in descending order of magnitude. We found that CPRL values with larger magnitudes are more stable than the original ResNet. This is because we use PNS optimization to give larger values a higher perceptual correlation score, and non-perceptual perturbations have less impact on this part.

extend our approach in our future work.

## References

- [1] Zeyuan Allen-Zhu and Yuanzhi Li. Feature purification: How adversarial training performs robust deep learning. In *2021 IEEE 62nd Annual Symposium on Foundations of Computer Science (FOCS)*, pages 977–988. IEEE, 2022. 1, 2
- [2] Jacob Benesty, Jingdong Chen, Yiteng Huang, and Israel Cohen. Pearson correlation coefficient. In *Noise reduction in speech processing*, pages 1–4. Springer, 2009. 6
- [3] Sebastian Bosse, Dominique Maniry, Klaus-Robert Müller, Thomas Wiegand, and Wojciech Samek. Deep neural networks for no-reference and full-reference image qual-



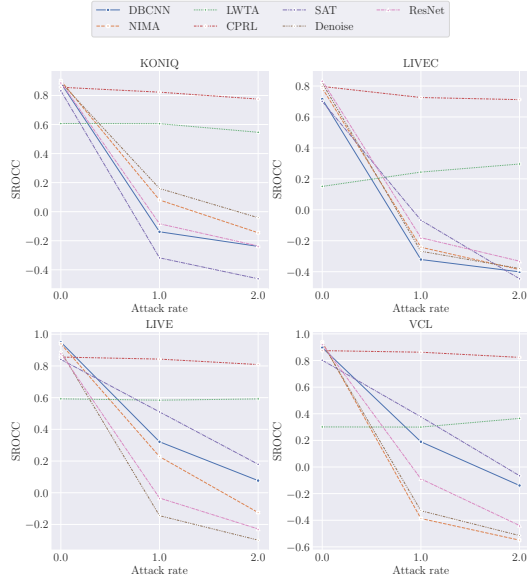


Figure 6. The SRCC result of the defence models under different FGSM attack rate with clean training.

ity assessment. *IEEE Transactions on image processing*, 27(1):206–219, 2017. 2

- [4] Hengrui Cai, Yixin Wang, Michael Jordan, and Rui Song. On learning necessary and sufficient causal graphs. *arXiv preprint arXiv:2301.12389*, 2023. 3
- [5] Moustapha Cisse, Piotr Bojanowski, Edouard Grave, Yann Dauphin, and Nicolas Usunier. Parseval networks: Improving robustness to adversarial examples. In *International Conference on Machine Learning*, pages 854–863. PMLR, 2017. 2
- [6] Logan Engstrom, Andrew Ilyas, Shibani Santurkar, Dimitris Tsipras, Brandon Tran, and Aleksander Madry. Adversarial robustness as a prior for learned representations. *arXiv preprint arXiv:1906.00945*, 2019. 2
- [7] Yuming Fang, Kede Ma, Zhou Wang, Weisi Lin, Zhijun Fang, and Guangtao Zhai. No-reference quality assessment of contrast-distorted images based on natural scene statistics. *IEEE Signal Processing Letters*, 22(7):838–842, 2014. 2
- [8] Deepti Ghadiyaram and Alan C Bovik. Massive online crowdsourced study of subjective and objective picture quality. *IEEE Transactions on Image Processing*, 25, 2015. 6
- [9] Ian J. Goodfellow, Jonathon Shlens, and Christian Szegedy. Explaining and harnessing adversarial examples, Mar. 2015. 2
- [10] Ian J. Goodfellow, Jonathon Shlens, and Christian Szegedy. Explaining and harnessing adversarial examples. *arXiv:1412.6572 [cs, stat]*, Mar. 2015. 2
- [11] Kaiming He, Xiangyu Zhang, Shaoqing Ren, and Jian Sun. Deep residual learning for image recognition. In *Proceedings of the IEEE conference on computer vision and pattern recognition*, pages 770–778, 2016. 2, 6
- [12] Andrew Ilyas, Shibani Santurkar, Dimitris Tsipras, Logan Engstrom, Brandon Tran, and Aleksander Madry. Adversarial examples are not bugs, they are features. *Advances in*

*neural information processing systems*, 32, 2019. 1, 2

- [13] Jean Kaddour, Aengus Lynch, Qi Liu, Matt J Kusner, and Ricardo Silva. Causal machine learning: A survey and open problems. *arXiv preprint arXiv:2206.15475*, 2022. 1, 3
- [14] James W Kalat. *Biological psychology*. Cengage Learning, 2015. 1
- [15] Harini Kannan, Alexey Kurakin, and Ian Goodfellow. Adversarial logit pairing. *arXiv preprint arXiv:1803.06373*, 2018. 3
- [16] Junho Kim, Byung-Kwan Lee, and Yong Man Ro. Demystifying causal features on adversarial examples and causal inoculation for robust network by adversarial instrumental variable regression. In *Proceedings of the IEEE/CVF Conference on Computer Vision and Pattern Recognition*, pages 12302–12312, 2023. 3
- [17] Kun Kuang, Peng Cui, Hao Zou, Bo Li, Jianrong Tao, Fei Wu, and Shiqiang Yang. Data-driven variable decomposition for treatment effect estimation. *IEEE Transactions on Knowledge and Data Engineering*, 34(5):2120–2134, 2020. 3
- [18] Dingquan Li, Tingting Jiang, Weisi Lin, and Ming Jiang. Which has better visual quality: The clear blue sky or a blurry animal? *IEEE Transactions on Multimedia*, 21(5):1221–1234, 2018. 2
- [19] Hanhe Lin, Vlad Hosu, and Dietmar Saupe. Kadid-10k: A large-scale artificially distorted iqa database. In *2019 Eleventh International Conference on Quality of Multimedia Experience (QoMEX)*, pages 1–3. IEEE, 2019. 1
- [20] Haoyang Liu, Maheep Chaudhary, and Haohan Wang. Towards trustworthy and aligned machine learning: A data-centric survey with causality perspectives. *arXiv preprint arXiv:2307.16851*, 2023. 1, 3
- [21] Fangrui Lv, Jian Liang, Shuang Li, Bin Zang, Chi Harold Liu, Ziteng Wang, and Di Liu. Causality inspired representation learning for domain generalization. In *Proceedings of the IEEE/CVF Conference on Computer Vision and Pattern Recognition*, pages 8046–8056, 2022. 3
- [22] Jupo Ma, Jinjian Wu, Leida Li, Weisheng Dong, Xuemei Xie, Guangming Shi, and Weisi Lin. Blind image quality assessment with active inference. *IEEE Transactions on Image Processing*, 30:3650–3663, 2021. 1, 2
- [23] Kede Ma, Wentao Liu, Tongliang Liu, Zhou Wang, and Dacheng Tao. dipiq: Blind image quality assessment by learning-to-rank discriminable image pairs. *IEEE Transactions on Image Processing*, 26(8):3951–3964, 2017. 2
- [24] Aleksander Madry, Aleksandar Makelov, Ludwig Schmidt, Dimitris Tsipras, and Adrian Vladu. Towards deep learning models resistant to adversarial attacks. *arXiv preprint arXiv:1706.06083*, 2017. 6
- [25] Xiongkuo Min, Guangtao Zhai, Ke Gu, Yutao Liu, and Xiaokang Yang. Blind image quality estimation via distortion aggravation. *IEEE Transactions on Broadcasting*, 64(2):508–517, 2018. 2
- [26] Xiongkuo Min, Guangtao Zhai, Ke Gu, Yucheng Zhu, Jiantao Zhou, Guodong Guo, Xiaokang Yang, Xinping Guan, and Wenjun Zhang. Quality evaluation of image de-hazing methods using synthetic hazy images. *IEEE Transactions on Multimedia*, 21(9):2319–2333, 2019. 1
- [27] Anish Mittal, Rajiv Soundararajan, and Alan C Bovik. Mak-

- ing a “completely blind” image quality analyzer. *IEEE Signal processing letters*, 20(3):209–212, 2012. 2
- [28] Takeru Miyato, Toshiki Kataoka, Masanori Koyama, and Yuichi Yoshida. Spectral normalization for generative adversarial networks. *arXiv preprint arXiv:1802.05957*, 2018. 5
- [29] Konstantinos P Panousis, Sotirios Chatzis, and Sergios Theodoridis. Stochastic local winner-takes-all networks enable profound adversarial robustness. *arXiv preprint arXiv:2112.02671*, 2021. 6
- [30] Judea Pearl. *Causality*. Cambridge university press, 2009. 4
- [31] Chongli Qin, James Martens, Sven Gowal, Dilip Krishnan, Krishnamurthy Dvijotham, Alhussein Fawzi, Soham De, Robert Stanforth, and Pushmeet Kohli. Adversarial robustness through local linearization. *Advances in Neural Information Processing Systems*, 32, 2019. 2
- [32] Hamid R Sheikh, Muhammad F Sabir, and Alan C Bovik. A statistical evaluation of recent full reference image quality assessment algorithms. *IEEE TIP*, 15(11):3440–3451, 2006. 6
- [33] Zheyang Shen, Peng Cui, Kun Kuang, Bo Li, and Peixuan Chen. Causally regularized learning with agnostic data selection bias. In *Proceedings of the 26th ACM international conference on Multimedia*, pages 411–419, 2018. 3
- [34] Baifeng Shi, Dinghuai Zhang, Qi Dai, Zhanxing Zhu, Yadong Mu, and Jingdong Wang. Informative dropout for robust representation learning: A shape-bias perspective. In *International Conference on Machine Learning*, pages 8828–8839. PMLR, 2020. 2
- [35] Elizabeth A Stuart. Matching methods for causal inference: A review and a look forward. *Statistical science: a review journal of the Institute of Mathematical Statistics*, 25(1):1, 2010. 3
- [36] Christian Szegedy, Wojciech Zaremba, Ilya Sutskever, Joan Bruna, Dumitru Erhan, Ian Goodfellow, and Rob Fergus. Intriguing properties of neural networks, Feb. 2014. 2
- [37] Hossein Talebi and Peyman Milanfar. Nima: Neural image assessment. *IEEE transactions on image processing*, 27(8):3998–4011, 2018. 6
- [38] Kaihua Tang, Mingyuan Tao, and Hanwang Zhang. Adversarial visual robustness by causal intervention. *arXiv preprint arXiv:2106.09534*, 2021. 3
- [39] Jin Tian and Judea Pearl. Probabilities of causation: Bounds and identification. *Annals of Mathematics and Artificial Intelligence*, 28(1-4):287–313, 2000. 2
- [40] Dimitris Tsipras, Shibani Santurkar, Logan Engstrom, Alexander Turner, and Aleksander Madry. Robustness may be at odds with accuracy. *arXiv preprint arXiv:1805.12152*, 2018. 2
- [41] Lei Wang, Qingbo Wu, King Ng Ngan, Hongliang Li, Fanman Meng, and Linfeng Xu. Blind tone-mapped image quality assessment and enhancement via disentangled representation learning. In *2020 Asia-Pacific Signal and Information Processing Association Annual Summit and Conference (AP-SIPA ASC)*, pages 1096–1102. IEEE, 2020. 2
- [42] Yixin Wang and Michael I Jordan. Desiderata for representation learning: A causal perspective. *arXiv preprint arXiv:2109.03795*, 2021. 2, 3, 5
- [43] Zhou Wang and Alan C Bovik. Reduced-and no-reference image quality assessment. *IEEE Signal Processing Magazine*, 28(6):29–40, 2011. 2
- [44] Zhou Wang, Alan C Bovik, Hamid R Sheikh, and Eero P Simoncelli. Image quality assessment: from error visibility to structural similarity. *IEEE transactions on image processing*, 13(4):600–612, 2004. 1, 2
- [45] Cihang Xie, Mingxing Tan, Boqing Gong, Alan Yuille, and Quoc V Le. Smooth adversarial training. *arXiv preprint arXiv:2006.14536*, 2020. 6
- [46] Cihang Xie, Yuxin Wu, Laurens van der Maaten, Alan L Yuille, and Kaiming He. Feature denoising for improving adversarial robustness. In *Proceedings of the IEEE/CVF conference on computer vision and pattern recognition*, pages 501–509, 2019. 1, 2, 6
- [47] Weilin Xu, David Evans, and Yanjun Qi. Feature squeezing: Detecting adversarial examples in deep neural networks. *arXiv preprint arXiv:1704.01155*, 2017. 2
- [48] Mengyue Yang, Xinyu Cai, Furui Liu, Weinan Zhang, and Jun Wang. Specify robust causal representation from mixed observations. In *Proceedings of the 29th ACM SIGKDD Conference on Knowledge Discovery and Data Mining*, pages 2978–2987, 2023. 3
- [49] Mengyue Yang, Zhen Fang, Yonggang Zhang, Yali Du, Furui Liu, Jean-Francois Ton, and Jun Wang. Invariant learning via probability of sufficient and necessary causes. *arXiv preprint arXiv:2309.12559*, 2023. 2, 3, 5
- [50] Junyong You and Jari Korhonen. Transformer for image quality assessment. In *2021 IEEE International Conference on Image Processing (ICIP)*, pages 1389–1393. IEEE, 2021. 2
- [51] Jerrold H Zar. Spearman rank correlation. *Encyclopedia of biostatistics*, 7, 2005. 6
- [52] Andela Zaric, Nenad Tatalovic, Nikolina Brajkovic, Hrvoje Hlevnjak, Matej Loncaric, Emil Dumic, and Sonja Grgic. Vcl@fer image quality assessment database. In *Proceedings ELMAR-2011*, pages 105–110. IEEE, 2011. 6
- [53] Guangtao Zhai and Xiongkuo Min. Perceptual image quality assessment: a survey. *Science China Information Sciences*, 63(11):1–52, 2020. 1
- [54] Bohang Zhang, Du Jiang, Di He, and Liwei Wang. Rethinking lipschitz neural networks and certified robustness: A boolean function perspective. *Advances in Neural Information Processing Systems*, 35:19398–19413, 2022. 2
- [55] Weixia Zhang, Dingquan Li, Xiongkuo Min, Guangtao Zhai, Guodong Guo, Xiaokang Yang, and Kede Ma. Perceptual attacks of no-reference image quality models with human-in-the-loop. *Advances in Neural Information Processing Systems*, 35:2916–2929, 2022. 1
- [56] Weixia Zhang, Kede Ma, Jia Yan, Dexiang Deng, and Zhou Wang. Blind image quality assessment using a deep bilinear convolutional neural network. *IEEE Transactions on Circuits and Systems for Video Technology*, 30(1):36–47, 2018. 2, 6
- [57] Wenbo Zhang, Tong Wu, Yunlong Wang, Yong Cai, and Hengrui Cai. Towards trustworthy explanation: On causal rationalization. *arXiv preprint arXiv:2306.14115*, 2023. 3
- [58] Xingxuan Zhang, Peng Cui, Renzhe Xu, Linjun Zhou, Yue He, and Zheyang Shen. Deep stable learning for out-of-distribution generalization. In *Proceedings of the IEEE/CVF*

- Conference on Computer Vision and Pattern Recognition*, pages 5372–5382, 2021. 3
- [59] Yonggang Zhang, Mingming Gong, Tongliang Liu, Gang Niu, Xinmei Tian, Bo Han, Bernhard Schölkopf, and Kun Zhang. Causaladv: Adversarial robustness through the lens of causality. *arXiv preprint arXiv:2106.06196*, 2021. 3